

# Fate of Springtime Atmospheric Reactive Mercury: Concentrations and Deposition at Zeppelin, Svalbard

Stefan Osterwalder,\* Sarah M. Dunham-Cheatham, Beatriz Ferreira Araujo, Olivier Magand, Jennie L. Thomas, Foteini Baladima, Katrine Aspomo Pfaffhuber, Torunn Berg, Lei Zhang, Jiaoyan Huang, Aurélien Dommergue, Jeroen E. Sonke, and Mae Sexauer Gustin



Cite This: *ACS Earth Space Chem.* 2021, 5, 3234–3246



Read Online

ACCESS |



Metrics & More



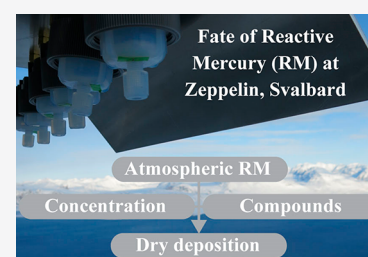
Article Recommendations



Supporting Information

**ABSTRACT:** Mid-latitude atmospheric elemental mercury (Hg) emissions undergo extensive oxidation to reactive Hg (RM) compounds during Arctic polar sunrise, resulting in enhanced atmospheric deposition that impacts Arctic marine wildlife and humans. It has been difficult to estimate RM dry deposition, because RM concentrations, compounds, and their deposition velocities are ill-defined. Here, we investigate RM concentrations sampled with membrane-based methods and find these to exceed denuder-based RM detection by 5 times at the Zeppelin Observatory on Svalbard (March 26–July 24, 2019). Measured dry deposition of gaseous oxidized Hg was about half of the modeled RM deposition, demonstrating that particulate-bound Hg was an important component of dry deposition. Using thermal membrane desorption, RM chemistry was found to be dominated by Hg–Cl/Br (51%) and Hg–N (45%) compounds. Back-trajectory analysis indicated that Hg–Br/Cl compounds were predominantly advected from within the marine boundary layer (sea ice exposure), while Hg–N originated from the free troposphere. Weekly average RM compound-specific dry deposition velocities ranged from 0.12 to 0.49 cm s<sup>-1</sup>, with a net RM dry deposition of 1.9 μg m<sup>-2</sup> (1.5–2.5 μg m<sup>-2</sup>; 95% confidence interval) that exceeds the mean annual Hg wet deposition flux in Svalbard. Overall, we find that springtime atmospheric RM deposition has been underestimated in the Arctic marine environment.

**KEYWORDS:** *Aerohead, Arctic, pollution, RMAS, speciation, thermal desorption*



## 1. INTRODUCTION

Mercury (Hg) pollution in the Arctic is of concern, because indigenous people rely heavily on marine-based diets that expose them to neurotoxic methylmercury.<sup>1,2</sup> Globally, the toxic burden of anthropogenic Hg pollution for human and ecosystem health is accepted by policy makers and has resulted in the United Nations Environment Programme (UNEP) Minamata Convention that aims to reduce human and ecosystem exposure to Hg.<sup>3</sup> However, to evaluate the effectiveness of the convention, we must improve our understanding on how Hg cycles between air, land, water, ice, and snow, especially in vulnerable ecosystems, such as the Arctic.<sup>4</sup> The uncertainty in estimates of atmospheric Hg deposition as gaseous elemental Hg (GEM), gaseous oxidized Hg (GOM), or particulate-bound Hg (PBM) to the Arctic Ocean is illustrated by a comparison of two global numerical Hg models. The GEOS-Chem model<sup>4</sup> suggested an atmospheric Hg input to the Arctic Ocean of 76 Mg year<sup>-1</sup>, while the GRAHM model estimated 108 Mg year<sup>-1</sup>.<sup>5</sup>

The discovery of coastal springtime atmospheric Hg depletion events (AMDEs) in 1995 indicated that reactive Hg (RM = GOM + PBM) dry deposition was an important pathway for atmospheric Hg inputs to Arctic marine ecosystems.<sup>6</sup> Subsequent studies suggested that, during AMDEs, about 100 Mg of RM year<sup>-1</sup> was deposited to Arctic

snow and ice.<sup>7,8</sup> Oxidation of GEM to GOM during AMDEs is primarily induced by photochemical activation of sea ice-derived halogen compounds.<sup>8,9</sup> In particular, bromine oxide and atomic bromine radicals (BrO<sub>x</sub>, BrO, and Br•) lead to the destruction of ozone (O<sub>3</sub>) and oxidation of GEM, with subsequent depletion of both GEM and O<sub>3</sub> in the Arctic atmosphere during polar sunrise.<sup>10,11</sup> Most recently, Obrist et al.<sup>12</sup> found that RM dry deposition to the coastal Arctic tundra was substantial during springtime AMDEs, depositing 0.8–2.8 μg m<sup>-2</sup> year<sup>-1</sup>. Dry deposition of RM during AMDEs results in higher total Hg concentrations in snow<sup>13,14</sup> that can be followed by re-emission of Hg<sup>0</sup> after photoreduction.<sup>2,15,16</sup> Approximately 90% of total Hg in snow can be re-emitted back to the atmosphere after AMDEs.<sup>1</sup>

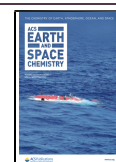
To assess the total input of Hg to Arctic ecosystems during AMDEs, it is crucial to improve RM dry deposition estimates. This could be done by measuring ambient RM concentrations

Received: August 25, 2021

Revised: September 28, 2021

Accepted: September 28, 2021

Published: October 18, 2021



and applying the values in dry deposition models or identifying RM compounds in ambient air and applying compound-specific deposition velocity calculations based on local meteorological data. The spatial resolution of Arctic RM measurements is limited, and the widely used measurement technique to quantify atmospheric Hg [Tekran speciation system (Tekran 2537/1130/1135), Tekran Instrument Corp., Ontario, Canada] has been demonstrated to underestimate RM by a factor of 2–13 in the planetary boundary layer<sup>17–24</sup> and by a factor of 1.6 in the free troposphere.<sup>25</sup> Other studies suggest that measurement artifacts for PBM are generated by temperature and collection time.<sup>26–28</sup> Selective collection and analysis of particles smaller than 2.5  $\mu\text{m}$  diameter with Tekran also raise the question of the possible underestimation of PBM concentrations,<sup>29</sup> particularly in oceanic environments, where the RM compounds are dominantly associated with larger (2–10  $\mu\text{m}$ ) marine aerosols.<sup>30,31</sup>

The Reactive Mercury Active System 2.0 (RMAS) of the University of Nevada, Reno, with cation-exchange membranes (CEMs) and nylon membranes<sup>32</sup> in combination with a down-facing aerodynamic sampler housing that also uses CEMs (Aerohead sampler),<sup>33,34</sup> has been shown to improve RM concentration measurements and GOM and RM dry deposition estimates, respectively, relative to the Tekran 2537/1130/1135 system.<sup>35</sup> These measurement methods have never been applied in the Arctic, although they are necessary because a low bias in RM deposition would lead to underestimation of Hg transfer from the atmosphere to marine and terrestrial ecosystems during AMDEs. Using the RMAS, the chemistry of RM compounds can be suggested using thermal desorption of nylon membranes and subsequent peak deconvolution.<sup>20,21,32,36</sup> This methodology allows for understanding if specific compounds, namely, HgO, Hg–Br/Cl (e.g., HgBr<sub>2</sub> and HgCl<sub>2</sub>), Hg–nitrogen [e.g., Hg(NO<sub>3</sub>)<sub>2</sub>], and Hg–sulfur (e.g., HgSO<sub>4</sub>) as well as some organic-bound compounds (e.g., MeHg),<sup>24</sup> are present. Knowledge about the chemistry of RM improved local estimates of RM deposition at a coastal research site in Florida, U.S.A.<sup>36</sup> Estimates of dry deposition were based on compound-specific deposition velocity calculations using a multiple resistance model that was developed by Zhang et al.<sup>37</sup> and modified by Lyman et al.<sup>33</sup>

Explaining the bias in the atmospheric RM concentration among different measurement methods in combination with better identification of chemical compounds of RM has been identified as a top priority task to improve the determination of RM dry deposition from local to global scales.<sup>18</sup> Here, we present a procedure to determine RM compound-specific dry deposition velocities to calculate springtime RM dry deposition in the Ny-Ålesund area on Svalbard. The goals of the study were to (1) intercompare RM concentrations using automated (Tekran) and manual methods (RMAS), (2) identify RM compounds by thermal desorption procedures, (3) investigate the source of RM compounds using back-trajectory analysis, and (4) calculate RM compound-specific dry deposition velocities and compare them to dry deposition measurements made by the Aerohead sampler. The incorporation of new observations of RM concentration, chemistry, and compound-specific dry deposition velocities is a necessary intermediate step toward substantially improving numerical models of Hg cycling in the Arctic.

## 2. MATERIALS AND METHODS

**2.1. Location and Sampling.** Air measurements were carried out from March 26 (11:00) to July 24 (08:00), 2019, at the Zeppelin Observatory (Zeppelin), located on Svalbard in the Norwegian Arctic. The atmospheric research and monitoring station was located on Zeppelin Mountain at 474 m above sea level (asl) (78.90° N, 11.88° E). The observatory was situated far from major air pollution sources and, thus, was within an undisturbed Arctic environment. A steep downhill slope faced north toward the research village of Ny-Ålesund, a small settlement with 35–185 inhabitants at 2 km from the sampling site. The station was operated by the Norwegian Institute for Air Research (NILU) in close collaboration with the Norwegian Polar Institute (NPI). Air inlets for all air Hg measurements were installed 3 m above ground in close proximity to one another, facing downward and toward the predominant wind direction (ESE). Automated atmospheric Hg measurements were carried out by the Norwegian University of Science and Technology (NTNU) in collaboration with NILU; manual sampling for RM analyzes was performed by NPI staff. Previous analysis of automated atmospheric Hg and snow Hg measurements at Zeppelin were reported by Dommergue et al.,<sup>13</sup> Berg et al.,<sup>38–40</sup> Aspö et al.,<sup>41</sup> Gauchard et al.,<sup>42</sup> Sprovieri et al.,<sup>43,44</sup> Sommar et al.,<sup>45</sup> Ferrari et al.,<sup>46</sup> Steen et al.,<sup>47</sup> and Angot et al.<sup>48</sup>

**2.2. Automated GEM and RM Measurements.** During the campaign, Tekran measured GEM, GOM, and PBM continuously, following methods briefly described in section S1 of the Supporting Information and detailed by Landis et al.<sup>49</sup> The only deviation from the standard operation procedures<sup>50,51</sup> was calculating GOM with the flush blank concentrations added to the GOM measurement; this was performed because adding the Tekran flush blank to RM (GOM + PBM) measurements resulted in a good agreement with manual RM measurements using polyethersulfone (PES) membranes at the high-altitude Pic du Midi Observatory.<sup>25</sup>

**2.3. Manual RM Measurements.** Three different sorption surface materials were used to sample RM. A PES membrane (47 mm diameter, 0.45  $\mu\text{m}$  pore size, Millipore) was previously applied<sup>25,52</sup> and showed similar sorption capacity and background Hg contents to CEM.<sup>53</sup> The PES and CEM (PES backbone that has been proprietarily treated, 47 mm diameter, 0.8  $\mu\text{m}$  pore size, Mustang-S, Pall Corporation) were applied extensively in recent studies (e.g., Gustin et al.,<sup>19</sup> Maruszczak et al.,<sup>25</sup> Luippold et al.,<sup>32</sup> and Miller et al.<sup>54</sup>) and were deemed the preferable material for quantitative RM measurements as a result of the high RM sorption efficiency.<sup>53</sup> Nylon membranes (47 mm diameter, 0.2  $\mu\text{m}$  pore size, Sartorius Stedium) were used to determine the chemistry of RM using thermal desorption procedures.<sup>19,24</sup> The chemistry of the RM compounds captured on the nylon membranes was determined by comparing membrane Hg desorption profiles from Svalbard to those developed for standard Hg compounds (see section 2.4 also).

**2.3.1. PES Measurements.** The PES sampling configuration captured RM in ambient air by pumping at 1 L min<sup>-1</sup> (membrane vacuum pump, KNF) through a one-stage outdoor filter pack protected from snow fall. The airflow was regulated by a ball flow meter (Fisher Scientific) and quantified with a digital volume meter (Siargo, Ltd.). The flow was regularly checked with a Bios Defender calibration unit and considered stable throughout the campaign. In the laboratory, the RM

content on PES after digestion was determined using a Brooks Rand Model III cold vapor atomic fluorescence spectrometer (CVAFS). The method detection limit (MDL) was 5 pg of Hg.<sup>25</sup> Details on RM analysis are described in section S2 of the Supporting Information, and a data overview is given in section S3 of the Supporting Information. In total, eight blank membranes were collected from the jars that housed PES prior to deployment of the new samples. The mean Hg content on PES blanks was  $13 \pm 8$  pg ( $1\sigma$ ;  $n = 8$ ). The limit of detection (LOD) was 25 pg ( $3\sigma$  of blank). The lowest RM on PES was 333 pg, collected from June 4 to 11, 2019. The blank percentage compared to the median RM was 2% (ranged from 1 to 6%), and all samples were above the LOD.

**2.3.2. RMAS Membrane Total Hg Measurements.** The RMAS was used to collect RM on CEM and nylon membranes. The sampling procedures for CEM and nylon membranes and their blank treatments were identical. Previous studies showed that nylon membranes did not collect all ambient compounds with the same efficiency as CEMs,<sup>19,53</sup> that the RM chemistry was in good agreement with measurements of anions (e.g.,  $\text{Cl}^-$ ,  $\text{Br}^-$ , and  $\text{NO}_3^-$ ),<sup>24</sup> and that RM compounds sorbed to the membrane did not transform during storage and shipment.<sup>53</sup> For RM sampling, ambient air was drawn through six sampling ports ( $n = 3$ , CEM;  $n = 3$ , nylon membranes) at a flow rate of  $1.7 \pm 0.2$  L  $\text{min}^{-1}$ . The downstream membranes in the two-stage filter holders allowed for the capture of Hg that passed through the upstream membrane. A detailed description of the RMAS can be found in the study by Luippold et al.<sup>24</sup> Triplicate blank CEM and nylon membranes were collected from the same jars as those that held the sample membranes. CEM and downstream nylon membranes were digested and analyzed using CVAFS following United States Environmental Protection Agency (U.S. EPA) Method 1631, and upstream nylon membranes were thermally desorbed (section 2.4 and section S2 of the Supporting Information). The mean of the triplicate CEM blanks, collected weekly at the start of each deployment, was  $38 \pm 13$  pg ( $1\sigma$ ;  $n = 17$ ), and the mean nylon membrane blank Hg content was  $14 \pm 7$  pg ( $1\sigma$ ;  $n = 17$ ). All CEM samples were above the LOD of 38 pg ( $3\sigma$  of blank); the LOD was less than 5% of the median RM (785 pg). Median CEM breakthrough for all samples was 8% ( $n = 17$ ). The nylon membrane LOD was 20 pg ( $3\sigma$  of blank); the two last samples of the campaign (harvested on July 17 and 24, 2019) were below the LOD. The mean breakthrough on the nylon membrane was 2% ( $1\sigma$ ;  $n = 15$ ), excluding the samples below the LOD.

**2.4. RM Compounds.** Upstream nylon membranes were thermally desorbed to characterize and quantify RM compounds. The thermal desorption profiles for different RM compounds (section S4 of the Supporting Information) were compared to pure GOM compounds for which profiles have been developed, including HgO, HgBr<sub>2</sub>, HgCl<sub>2</sub>, HgN<sub>2</sub>O<sub>6</sub>, HgSO<sub>4</sub>, and elemental Hg, as well as methylmercury chloride directly added to membranes.<sup>20,21,36</sup> Thermal desorption profiles have been used to identify Hg compounds in not only ambient air, but also other matrices. Exemplarily, Biester and Scholz<sup>55</sup> developed profiles for solids that have peaks at similar locations as ours for similar compounds.

Individual RM compounds were identified from peak deconvolution of thermal desorption profiles.<sup>19,20,24,32</sup> Each profile was considered to follow a Gaussian distribution (section S3 of the Supporting Information) and was

deconvoluted on the basis of the curve-fitting function in MATLAB, version 2018a. Peak temperature ranges were defined for different compounds using an improved calibration system: 80–85 °C for [–O], 90–110 °C for [–Br/Cl], 125–135 °C for [–N], 150–155 °C for [–S], and 180–190 °C for methylmercury (MeHg) or generally organic Hg compounds.<sup>24,32</sup> To quantify the RM compounds on each nylon membrane, the integral of the area beneath each Gaussian peak was calculated ( $\text{pg m}^{-3} \text{ } ^\circ\text{C}$ ). The relative contribution of each RM compound was calculated on the basis of the integrated peak area. The percentage of the compounds was determined by dividing the concentration of the identified compound using thermal desorption data, specifically the area under the curve, by the total amount of RM measured. RM compound contribution collected on each nylon membrane was determined weekly on the basis of the peak deconvolution analysis. For details on the thermal desorption and peak deconvolution procedures, see the study by Luippold et al.<sup>32</sup>

**2.5. Back-Trajectory Modeling.** The Hybrid Single-Particle Lagrangian Integrated Trajectory model (HYSPPLIT, version 4.2.0), developed by the National Oceanic and Atmospheric Administration (NOAA),<sup>56</sup> was driven with 3 hourly meteorological input data from the Global Data Analysis System (GDAS; 1° latitude–longitude  $360 \times 181$  grid) to identify the potential source regions of RM compounds. The model was run in backward mode for 10 days every 2 h throughout the CEM and nylon membrane sampling periods at Zeppelin (474 m asl). In total, ~84 backward trajectories were calculated for each sampling period. The spatial (horizontal and vertical) residence times of the air masses were calculated. The back-trajectory model results were combined with five major surface categories, land (no snow cover), open water, permanent ice/snow, sea ice, and snow on land, determined using ESRI ArcGIS Pro (version 10.6), to provide the time series of percent surface exposure of particles along trajectories. Moreover, the percent of particles along trajectories that reside within the boundary layer (BL) and in the free troposphere (FT) was analyzed. Details on generation of surface maps and back-trajectory statistics are given in section S5 of the Supporting Information.

**2.6. GOM/RM Dry Deposition.** **2.6.1. Dry Deposition Measurements.** Three passive Aerohead samplers were deployed to measure GOM dry deposition<sup>33,34</sup> next to the inlets for the automated and manual RM samplers. GOM was collected on CEM (127 mm diameter, 0.8  $\mu\text{m}$  pore size, Mustang-S, Pall Corporation) on a weekly basis. After each deployment, the three CEM and two non-deployed blanks were collected. The samples were stored in 50 mL centrifuge tubes in double-zipper bags at  $-20$  °C. In the laboratory, the membranes were digested and analyzed identically to the CEM and nylon from the RMAS. Dry deposition of RM was calculated following Lyman et al.<sup>34</sup>

$$D = \frac{\left[ \frac{S - B}{A} \right]}{T} \quad (1)$$

where  $D$  is the deposition rate in  $\text{ng m}^{-2} \text{ h}^{-1}$ ,  $S$  is the mass of Hg on the membrane (ng),  $B$  is the mass of Hg on the method blanks (ng),  $A$  is the surface area of the membrane ( $0.0104 \text{ m}^2$ ), and  $T$  is the deployment duration (h). The mean of all Aerohead CEM blanks was  $166 \pm 112$  pg ( $1\sigma$ ;  $n = 35$ ). The GOM dry deposition MDL for a weekly deployment was  $0.29 \text{ ng m}^{-2} \text{ h}^{-1}$  (blank +  $3\sigma$ ). Uncertainty in the GOM dry

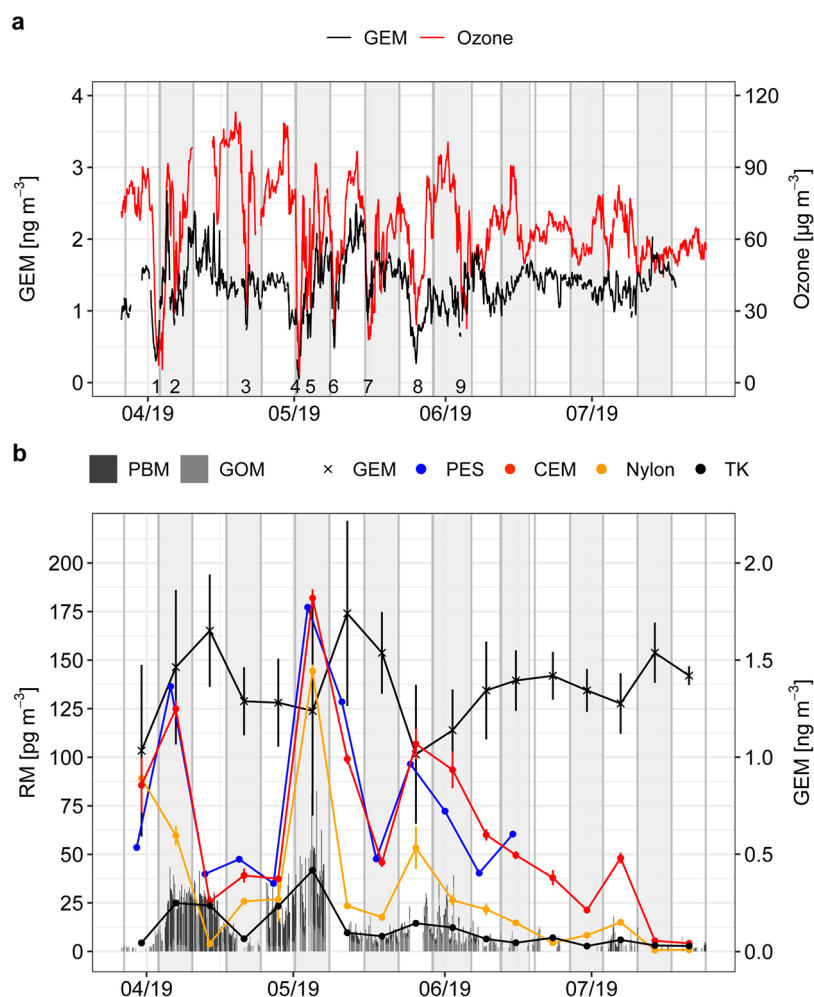


**Figure 1.** Time series of atmospheric Hg species and O<sub>3</sub> from March 26 to July 24, 2019. (a) GEM (black line) and O<sub>3</sub> (red line) concentrations are displayed as hourly means. AMDEs are indicated with numbers 1–9. (b) Mean concentration of GEM (black cross), RM on PES (blue dots), RM on CEM (red dots), and RM on nylon membranes (yellow dots). RM from Tekran (TK) measurements (black dots), as PBM and GOM measurements (gray bars), are also displayed. Error bars represent 1 $\sigma$  and are indicated where  $n \geq 3$ . PES, CEM, and nylon membranes were deployed for 1 week. Sampling periods for CEM and nylon membranes are indicated with alternate white and gray backgrounds. The weekly PES sampling was offset from CEM and nylon membrane by 1 day.

deposition measurements originates from the fact that we measure deposition on an artificial surface and not on snow, ice, or tundra vegetation directly, where GOM can be reduced and subsequently re-emitted to the atmosphere. The surface of the CEM provides physical means for understanding temporal changes of GOM dry deposition.<sup>34</sup>

**2.6.2. Dry Deposition Modeling.** Weekly dry deposition of RM was estimated in a three-step procedure. First, we determined the individual RM compounds [Hg(OH)<sub>2</sub>, HgBr<sub>2</sub>/HgCl<sub>2</sub>, HgN<sub>2</sub>O<sub>6</sub>, HgSO<sub>4</sub>, and MeHg] using thermal desorption and peak deconvolution procedures (section 2.4). Second, we calculated the RM compound-specific dry deposition velocity using a multi-resistance model.<sup>37</sup> The basic source code of the multi-resistance model was described by Lyman et al.<sup>33</sup> and was subsequently applied by Huang et al.<sup>36</sup> Here, the code was modified according to the description in section S6 of the Supporting Information and is publicly accessible ([https://github.com/JiaoyanHuang/Dry\\_Depo\\_multi\\_res\\_model](https://github.com/JiaoyanHuang/Dry_Depo_multi_res_model)). The meteorological model input parameters were derived from hourly ERA5 data, the fifth generation ECMWF atmospheric reanalysis of the global climate.<sup>57</sup> The meteorological data were representative for a 31 km grid

covering the area around Zeppelin. Snow depth was determined at two measurement stations, representing a lower and upper limit of snow depth in the area. The first station, representing low snow depth, was located on a measurement field just south of the Ny-Ålesund village, and the second station, Bayelva, was located about 3 km outside the village and represented the upper limit of snow depth.<sup>58</sup> Third, we multiplied the RM compound-specific dry deposition velocities (calculated by the model) with the relative percentage of the RM compound concentrations measured by Tekran or from CEM analysis.

**2.7. Uncertainty in RM Dry Deposition Modeling.** The uncertainty of the modeled RM dry deposition was assessed using the Monte Carlo simulation approach (Crystal Ball) and is reported as the 95% confidence interval of 10 000 simulations. The probability distributions of the key input parameters for the model were obtained using the “BatchFit” function in Crystal Ball based on the dataset for each sampling period. Normal distribution and log-normal distribution were chosen for distribution fitting, and the  $p$  values for the significance levels of the fitted distributions were all <0.05. The uncertainty analysis, however, does not include the issues of

(1) lower sorption efficiency (ca. 50%) of RM on nylon membranes compared to CEMs and (2) that, during peak deconvolution, mixed compounds, e.g., HgBrNO<sub>3</sub>, are not well-defined. To minimize these uncertainties, the nylon membranes were not used as a quantitative sorption surface, but for RM compound analysis only. Several studies have confirmed that nylon membranes sorbed Hg–Br and Hg–Cl compounds linearly with increasing concentrations (under ambient and laboratory conditions),<sup>22,53</sup> and these compounds were neither lost nor transformed RM during sampling and storage.<sup>53</sup> However, CEM collected systematically higher concentrations of HgBr<sub>2</sub>, HgCl<sub>2</sub>, and a HgO compound.<sup>21</sup> More recent work has demonstrated that the nylon membranes do not effectively collect Hg–N compounds.<sup>20</sup> We are learning incrementally about the use of the membrane for identifying the chemistry of the compounds. The thermal desorption and peak deconvolution procedure introduces uncertainty, because there are only a limited number of RM compounds for which calibration profiles can be developed, and currently, the desorption profiles are broad. However, comparing the chemistry of the compounds to oxidants measured or expected in the air for a variety of locations as well as ion chromatography measurement of ions on the nylon membranes supports the RM chemistry observed. For example, in Hawaii, halogenated compounds were dominant, while in Nevada, adjacent to a highway, N–S–O Hg compounds were present, and in a forested area in Maryland, organic compounds were measured.<sup>24</sup> This indicates that we are effectively getting at the compounds in general, although we do not know the exact chemistry. More work needs to be done to quantify the chemistry and develop surfaces that are better at retaining compounds.

**2.8. Auxiliary Variables.** Meteorological parameters from Zeppelin, including the air temperature, wind speed, wind direction, relative humidity, and atmospheric pressure, were provided with an hourly resolution by NILU. Hourly means of tropospheric O<sub>3</sub> concentrations were measured by NILU using an ultraviolet (UV) absorption spectrometer (API 400A). Hourly means of particulate matter concentrations (PM<sub>2.5</sub>, PM<sub>10</sub>, and PM<sub>total</sub>) were derived from a FIDAS 200S instrument (Palas GmbH, Germany) operated by Stockholm University (SU). Daily means of particulate and gaseous nitrogen compounds (HNO<sub>3</sub>/NO<sub>3</sub><sup>−</sup> and NH<sub>4</sub><sup>+</sup>/NH<sub>3</sub>) were collected on a three-stage filter pack and analyzed using a Thermo Scientific Dionex Integrion HPLC system equipped with a Dionex AS9 column<sup>59</sup> and made available by NILU.

### 3. RESULTS AND DISCUSSION

**3.1. Quantification of Atmospheric Hg Using the Tekran System.** The mean GEM ± 1σ concentration measured between March 26 and July 24, 2019 was 1.36 ± 0.4 ng m<sup>−3</sup> (Figure 1a). During that period, nine distinct AMDEs were identified, with eight observed in April and May and one in early June. The occurrence of an AMDE was defined when GEM decreased below 1 ng m<sup>−3</sup><sup>41</sup> and the O<sub>3</sub> concentration dropped below the fifth percentile (33 μg m<sup>−3</sup>). An AMDE starts when the concentration of GEM sharply decreases and ends when GEM increases again to average concentrations. As a result of AMDEs, GEM concentrations in the Arctic are typically the lowest in April and May. From 2000 to 2009<sup>39</sup> and from 2011 to 2015,<sup>48</sup> 86 and 75%, respectively, of annual observed AMDEs occurred during the April and May time period. As a result of the influence of AMDEs during the

sampling campaign, the mean GEM concentration during the campaign (1.36 ng m<sup>−3</sup>) was lower than the annual mean of 1.54 ± 0.3 ng m<sup>−3</sup> measured between 2000 and 2009<sup>39</sup> and annual means ranging from 1.47 to 1.51 ng m<sup>−3</sup> between 2011 and 2015.<sup>48</sup> In summer, GEM increases as a result of re-emission of previously deposited Hg to surfaces and re-emission of surface Arctic Ocean dissolved Hg.<sup>60–62</sup>

Automated Tekran measurements of RM (GOM + PBM) for the whole sampling campaign were in the range of 2.6–13.1 pg m<sup>−3</sup> for GOM and 2.1–29.9 pg m<sup>−3</sup> for PBM (10th and 90th percentiles). The mean Tekran RM concentration (RM<sub>TK</sub>) was 14.6 ± 12.7 pg m<sup>−3</sup>, and the values spanned from below the MDL to 82.6 pg m<sup>−3</sup> (Figure 1b). During AMDEs, GOM and PBM concentrations were 9.6 and 20.5 pg m<sup>−3</sup>, on average, and elevated by 42 and 54%, respectively, compared to the entire campaign average. These values were at the lower end compared to those measured at Zeppelin during AMDEs in 2003<sup>41</sup> and in 2007–2008.<sup>47</sup> Overall, RM<sub>TK</sub> was <43.5 pg m<sup>−3</sup> (90th percentile) during AMDEs and lower (<30.8 pg m<sup>−3</sup>, 90th percentile) during the entire campaign.

#### 3.2. Quantification of RM Using Manual Methods.

The mean RM concentration sampled on CEM (RM<sub>CEM</sub>) was 63 ± 45 pg m<sup>−3</sup> (section S3 of the Supporting Information). The highest concentrations were found between May 1 and 8 (182 pg m<sup>−3</sup>), and the lowest concentrations were found at the end of the campaign from July 17 to 24 (4 pg m<sup>−3</sup>). The large variation among samples was due to the occurrence of AMDEs until the beginning of June (Figure 1b). Thereafter, RM<sub>CEM</sub> tended to decrease, with one exception from July 3 to 10 when RM<sub>CEM</sub> was 48 pg m<sup>−3</sup>. The RM concentration on PES (RM<sub>PES</sub>) was sampled until June 18, 2019 and was similar to RM<sub>CEM</sub>, even though the PES were replaced 1 day in advance compared to CEM (slope = 0.91; r<sup>2</sup> = 0.86; Figure S1a of the Supporting Information). The mean RM<sub>PES</sub> was 78 ± 46 pg m<sup>−3</sup>, similar to mean RM<sub>CEM</sub> concentrations for the same period to within 2% (March 26–June 18). The good agreement between the CEM and PES materials was previously demonstrated by Dunham-Cheatham et al.,<sup>53</sup> showing no significant difference between the two materials (α = 0.05). In concert with that study, the nylon membranes in this study were less efficient at capturing RM.

The mean RM concentration on nylon membranes (RM<sub>nylon</sub>) was 32 ± 37 pg m<sup>−3</sup>. The nylon membrane recovery was 50% (range from 12 to 104%) of the RM sorbed on CEM (Figure 1b). The lower RM content on nylon membranes was likely due to the different sorption efficiency of varying RM compounds to this material.<sup>19,20,24,36</sup> Despite the difference in captured RM, the relationship between RM<sub>CEM</sub> and RM<sub>nylon</sub> was fairly constant (r<sup>2</sup> = 0.75; p < 0.05; section S3 of the Supporting Information). This supports the conclusions from previous studies that nylon membranes are not suitable for quantitative RM concentrations but are suitable for thermal desorption analysis to identify RM compounds.<sup>19,53</sup>

Weekly mean RM<sub>CEM</sub> and RM<sub>PES</sub> were up to 19 and 22 times higher compared to RM<sub>TK</sub>, respectively (Figure S1b of the Supporting Information). On average, RM<sub>CEM</sub> was 5.3 times and RM<sub>PES</sub> was 5.2 times higher than RM<sub>TK</sub> based on weekly averages (11.8 ± 10.4 pg m<sup>−3</sup>). Tekran RM measurements were calculated as the sum of GOM and PBM concentrations and the amount of Hg released during the three 5 min flush cycles (flush<sub>TK1–3</sub>). The discrepancy between RM on membranes and RM<sub>TK</sub> agrees with recently performed comparisons, where RM on membranes was 2–13 times

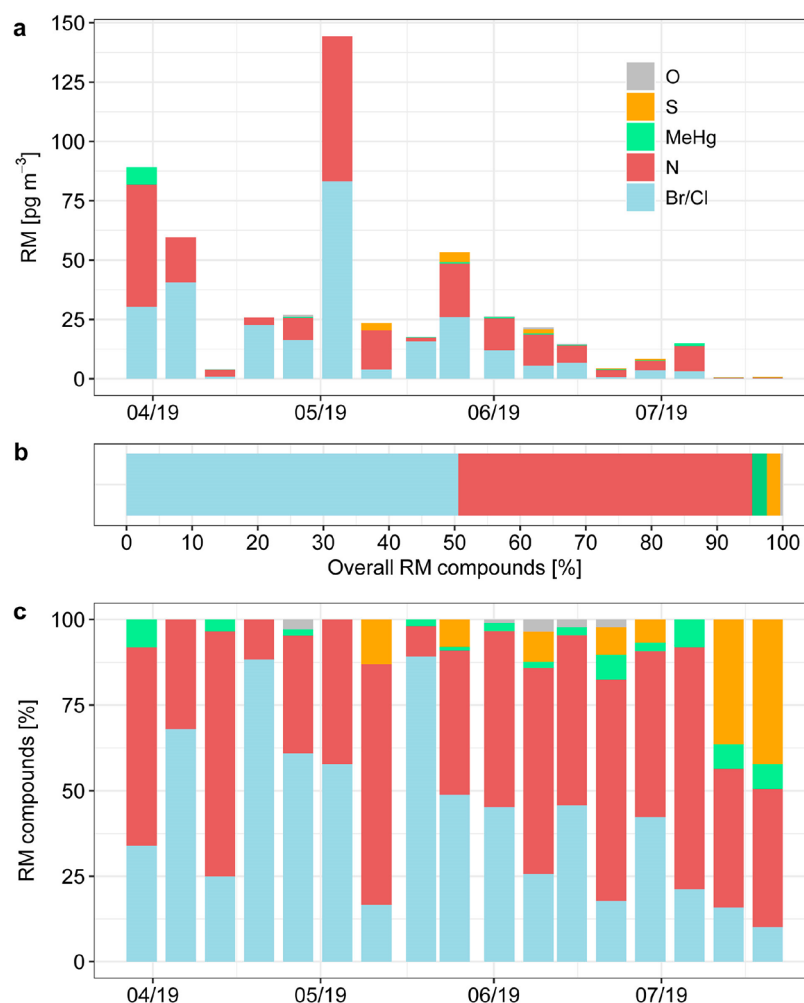


**Figure 2.** RM compounds determined from March 27 until July 24, 2019. (a) RM concentration on the nylon membrane from the RMA for a mixture of RM compounds identified by thermal desorption and peak deconvolution. The frequency distribution of RM compounds (%) is given for (b) entire campaign (mean) and (c) each sampling event.

greater.<sup>17,18,20–22</sup> However, we point out that the impactor on Tekran removes particles with aerodynamic diameters larger than  $2.5 \mu\text{m}$ , while the membrane-based systems might also capture particles of  $>2.5 \mu\text{m}$ . The mean  $\text{PM}_{2.5}$  concentration ( $0.97 \mu\text{g m}^{-3}$ ) was only 30% of the total mean PM concentration ( $3.29 \mu\text{g m}^{-3}$ ) measured during our campaign. Thus,  $\text{RM}_{\text{TK}}$  tends to be lower compared to membrane-based systems as a result of the lower efficiency of GOM collection<sup>63</sup> and the exclusion of large PBM ( $>2.5 \mu\text{m}$ ) from analysis. More multi-season  $\text{RM}_{\text{CEM}}$  and  $\text{RM}_{\text{PES}}$  time series at multiple Arctic sites are necessary to derive robust correlations with automated measurements and to potentially correct previous Tekran RM data.

**3.3. Compounds of RM.** Thermal desorption and peak deconvolution revealed the composition of RM species that were retained on the nylon membranes (section S4 of the Supporting Information). The weekly mean  $\text{RM}_{\text{nylon}}$  ranged from 1 to  $144 \text{ pg m}^{-3}$  (Figure 2a). The dominant RM compounds sampled over the course of the campaign were Hg–Br/Cl and Hg–N, which accounted for 51 and 45% of the total RM on nylon membranes, respectively (Figure 2b). Organic-based Hg compounds (e.g., MeHg) contributed 2% to the overall RM concentration. Sulfur compounds (Hg–S) accounted also for 2%, while the contribution of oxide

compounds (HgO) was  $<1\%$ . The relative contribution of the RM compounds was calculated each week throughout the campaign (Figure 2c). The Hg–Br/Cl compounds indicate reactions of GEM with halogens (Cl,  $\text{Cl}_2$ , Br,  $\text{Br}_2$ ) within the atmospheric BL,<sup>7</sup> where  $\text{Br}^\bullet$  is regarded as one of the primary first-step atmospheric oxidants to produce RM intermediates, such as  $\text{Hg}^{\text{I}}\text{Br}$ .<sup>11,64</sup> The occurrence of Hg–N compounds depends upon several different factors, such as N emission sources or atmospheric redox processes occurring between the source and receptor site.<sup>65–67</sup> Atmospheric  $\text{NO}_2$  radicals are also considered to be the dominant second-step oxidant transforming  $\text{Hg}^{\text{I}}\text{Br}$  to  $\text{Hg}^{\text{II}}\text{BrONO}$  in the free troposphere.<sup>64,68</sup> During the first sampling deployment week, RM was composed of 34% Hg–Br/Cl and 58% Hg–N compounds, but in contrast, during week 2, 68% Hg–Br/Cl and 32% Hg–N were detected. During week 6, when two AMDEs occurred and the largest RM concentrations were measured ( $182 \text{ pg m}^{-3}$ ), Hg–Br/Cl and Hg–N contributed similar parts to total RM (58 and 42%, respectively). During weeks 7 and 8, the dominant RM compound on the nylon membranes changed from Hg–N (70%) to Hg–Br/Cl (89%). To explain differences in chemical composition, we investigated the role of air mass exposure on the dominant RM

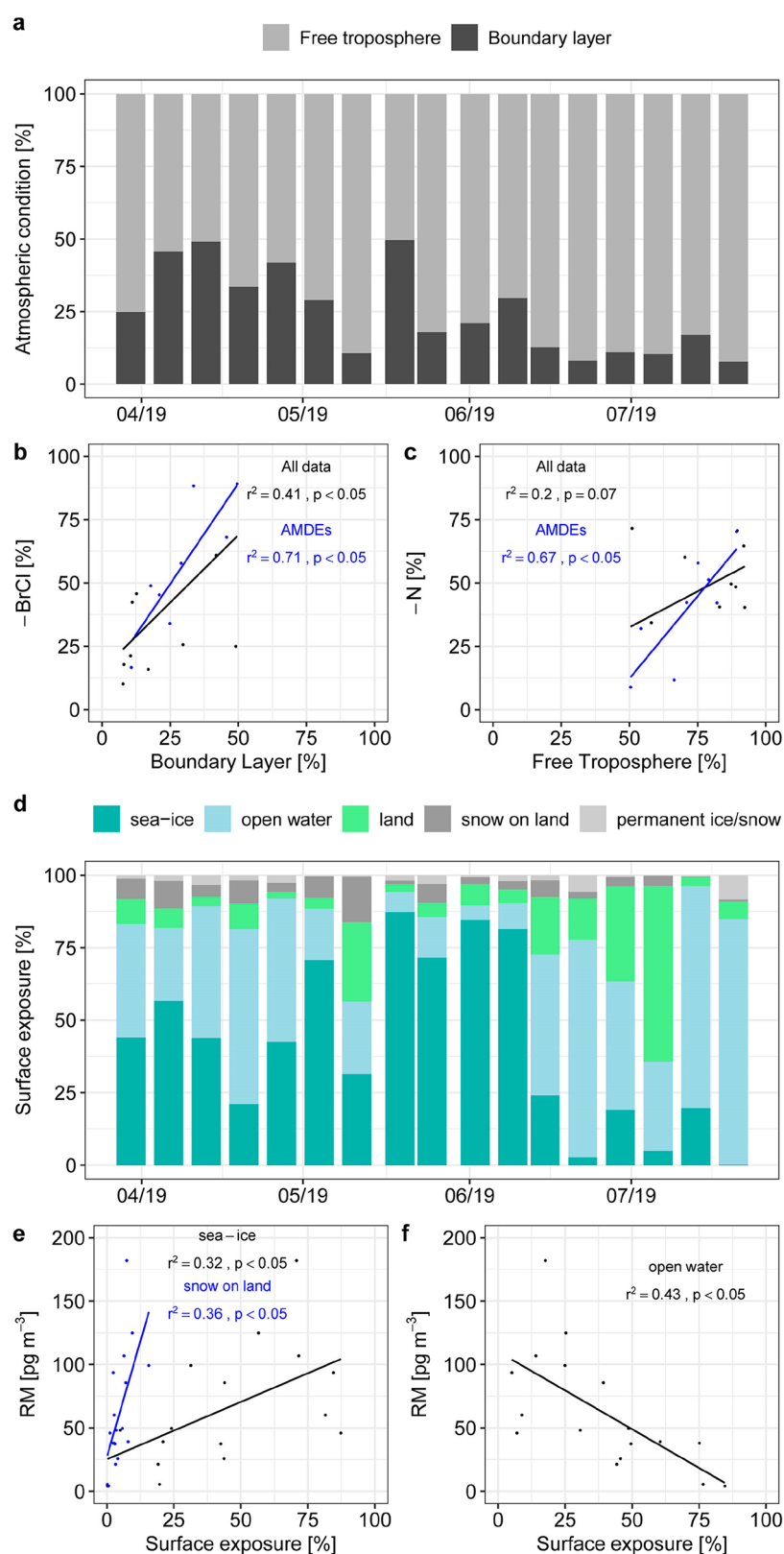


**Figure 3.** HYSPLIT simulation of air mass trajectory residence time in the atmosphere and exposure to surfaces. (a) Percentage of time that the trajectories were in the boundary layer (BL) and free troposphere (FT) for each of the 17 deployment periods. Linear correlation during the entire campaign and during weeks when AMDEs occurred between (b) Hg–Br/Cl and residence time in the BL and (c) Hg–N and residence time in the FT. (d) Surface exposure of trajectories to the five major surface categories: sea ice, open water, land (no snow), snow-covered land, and permanent ice and snow. Linear correlation between (e)  $RM_{CEM}$  and exposure to sea ice and snow-covered land and (f)  $RM_{CEM}$  and exposure to open water.

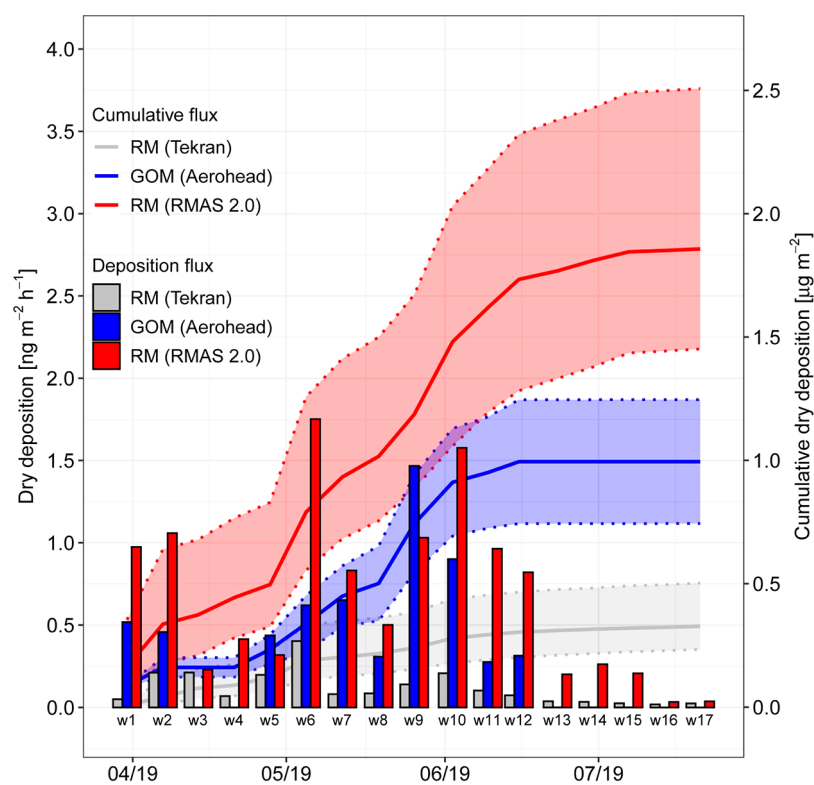


**Figure 4.** Measured GOM and modeled RM dry deposition for the entire sampling period. Weekly GOM dry deposition calculated on the basis of the Aerohead system (measured) and RM dry deposition estimated on the basis of the Tekran and RMAS systems using RM compound-specific dry deposition velocities (modeled). The cumulative flux over the entire sampling campaign (lines) and associated uncertainties (shaded area, 95% confidence interval) are given.

compounds, Hg–Br/Cl (51%) and Hg–N (45%), along the air mass back trajectory.

**3.4. Origin of RM.** To investigate if atmospheric conditions influence the RM compounds, the relationship between the trajectories within the BL and in the FT was analyzed. The percentage of time that the trajectories arriving at Zeppelin resided in the BL ranged from 7 to 50% (Figure 3a). There was a significant correlation between the percentage of time that the trajectories were within the BL and the determined percentage of Hg–Br/Cl compounds ( $r^2 = 0.4$ ;  $p < 0.05$ ). The relationship became even stronger during periods when AMDEs occurred ( $r^2 = 0.7$ ;  $p < 0.05$ ; Figure 3b). During the same period, Hg–N compounds occurred more frequently when the advected air mass originated from the FT ( $r^2 = 0.7$ ;  $p < 0.05$ ; Figure 3c). This indicates that air masses enriched in Hg–Br/Cl were in contact with the surface for longer periods compared to air masses enriched in Hg–N that were originating predominantly in the FT.

Air masses arriving at Zeppelin were mainly exposed to sea ice and open water (Figure 3d). The RM concentrations increased when air masses were exposed to sea ice ( $r^2 = 0.32$ ;  $p < 0.05$ ) or land covered by snow ( $r^2 = 0.36$ ;  $p < 0.05$ ; Figure 3e). Lower RM concentrations were measured when air masses were exposed to open water ( $r^2 = 0.43$ ;  $p < 0.05$ ; Figure 3f). The positive relationship between Hg–Br/Cl and the time that the air mass passed over sea ice ( $p = 0.06$ ; Figure S4 of the Supporting Information) further corroborates that sea ice and snow on sea ice are the main source of reactive halogen species in the Arctic that oxidize GEM. This can occur via one of two mechanisms: activation from snow on sea ice (surface snow source)<sup>69</sup> or lofted salty snow particles that form sea salt

aerosols within the BL (blowing snow particle source).<sup>70,71</sup> Although Hg–Br and Hg–Cl compounds are indistinguishable with our methods, all reactive halogen species in the atmosphere are produced from similar sources, i.e., snow on sea ice and BL aerosols.<sup>72–74</sup> In the atmosphere, both Br• and Cl• react with O<sub>3</sub> to form halogen oxides;<sup>75,76</sup> both halogen radicals and halogen oxides lead to the oxidation of GEM to RM.<sup>10</sup>

A weak positive relationship between Hg–N and the time that the air mass passed over land without snow cover ( $r^2 = 0.2$ ;  $p = 0.06$ ; Figure S4 of the Supporting Information) indicated an anthropogenic source of N compounds (i.e., NO<sub>2</sub>) from more densely populated areas further south or, more specifically, springtime transport of plumes from Asian industries or Siberian wildfires.<sup>77</sup> Emitted NO<sub>2</sub> leads to enhanced GEM oxidation and increased Hg–N concentrations downwind. Although more data are required (multi-seasonal sampling) to establish significant relationships between RM compounds and exposure time of air masses to different surface types, our conclusions are well-illustrated by comparing surface exposure during weeks 7 and 8. A maximum of Hg–N compounds was measured during week 7 (70% of total RM), when exposure time of air masses over land (43%) and the residence time in the FT (89%) were long. Back-trajectory analysis indicated that the air moved mainly from Fennoscandia (17%) and Siberia (74%) over the eastern Arctic Ocean to Zeppelin (Figure S5g of the Supporting Information). The Siberian air mass originated from areas where wildfires were ubiquitous between May 8 and 15, 2019 (<https://earthdata.nasa.gov/earth-observation-data/near-real-time/firms>). The mean BL height measured along the air mass

trajectories was 277 m asl and was elevated in comparison to week 8 (87 m asl). In week 8, Hg–Br/Cl was the dominant RM compound (89%) and air masses passed predominantly over sea ice (87%) from areas east of Zemlya Georga and northwest of Svalbard to Zeppelin (Figure S5h of the Supporting Information). The residence time of the air mass in the BL was 50%, which corresponded to the longest residence time in the BL among all weeks of sampling (Figure 3a). Thus, the comparatively long residence time of air masses within the BL over the sea ice-covered Arctic Ocean constituted the main source region of Hg–Br/Cl arriving at Zeppelin.

### 3.5. Dry Deposition Measurements and Modeling.

Mean local GOM dry deposition at Zeppelin measured by Aerohead samplers was  $0.35 \text{ ng m}^{-2} \text{ h}^{-1}$ , and weekly averages ranged from below the MDL to  $1.47 \text{ ng m}^{-2} \text{ h}^{-1}$  (Figure 4). Measurements of GOM dry deposition in 9 out of 17 weeks were above the MDL ( $0.29 \text{ ng m}^{-2} \text{ h}^{-1}$ ). The cumulative Aerohead GOM dry deposition measured from March 27 to July 24, 2019 was  $1 \mu\text{g m}^{-2}$ , with a 95% confidence interval ranging from 0.74 to  $1.25 \mu\text{g m}^{-2}$  (Figure 4). Dry deposition of GOM measured by Aerohead samplers was negligible (<0.1% of the cumulative flux) during the last 5 weeks of measurements (from June 19 to July 24, 2019). During weeks 3 and 4, there was less than 1 pg of GOM measured on the Aerohead CEM, in contrast to 795 pg analyzed on the CEMs from RMAS, indicating the importance of particulate-bound Hg. During weeks 5 and 9, measured GOM dry deposition exceeded the modeled RM dry deposition by 38 and 43%, respectively. A comparison of meteorological and chemical variables during these weeks with the preceding and following weeks indicated no unusual conditions. It could be that a compound was present that was sticking to the open-faced membranes in the Aeroheads but not making its way into the filter packs holding membranes in the RMAS or the compound had a higher deposition velocity than other compounds. This would be true for HgO that once formed is thought to become a particle and rapidly deposit to surfaces.<sup>78</sup> Thus, understanding reactions forming and the chemistry of compounds of GOM/RM is greatly needed.

The cumulative modeled dry deposition of RM based on RM compound-specific dry deposition velocities and  $\text{RM}_{\text{TK}}$  was  $0.33 \mu\text{g m}^{-2}$ , with a 95% confidence interval ranging from 0.23 to  $0.50 \mu\text{g m}^{-2}$  (Figure 4). The modeled flux was one-third of the measured flux. The average RM dry deposition velocities of  $\text{Hg}(\text{OH})_2$ ,  $\text{HgBr}_2/\text{HgCl}_2$ ,  $\text{HgN}_2\text{O}_6$ ,  $\text{HgSO}_4$ , and MeHg were very similar and differed by less than 5% during each sampling week (Table S6 of the Supporting Information). The dominant RM compounds  $\text{HgBr}_2/\text{HgCl}_2$  and  $\text{HgN}_2\text{O}_6$  both exhibited a mean deposition velocity of  $0.28 \pm 0.10 \text{ cm s}^{-1}$  over the course of the campaign. The weekly mean RM deposition velocities ranged from  $0.12 \text{ cm s}^{-1}$  (week 15) to  $0.48 \text{ cm s}^{-1}$  (week 10). The mean deposition velocity of all RM compounds was  $0.32 \pm 0.09 \text{ cm s}^{-1}$  when the area around Zeppelin was covered by snow, and  $0.21 \pm 0.08 \text{ cm s}^{-1}$  during the last 5 weeks of measurements when snowmelt had occurred (June 17, 2019).

The modeled cumulative dry deposition based on  $\text{RM}_{\text{CEM}}$  was  $1.86 \mu\text{g m}^{-2}$  with a 95% confidence interval ranging from 1.45 to  $2.50 \mu\text{g m}^{-2}$  (Figure 4). Thus, RM dry deposition was 5.6 times larger compared to estimates using Tekran data (Table S7 of the Supporting Information). The discrepancy between the measured (Aerohead) and modeled (RMAS)

cumulative dry deposition, a factor of 1.9, was due to the Aerohead sampling GOM, while PBM adsorbs negligibly to the down-facing surrogate surface as a result of gravity.<sup>22,34–36,79–81</sup> The inconsistency during weeks 1, 2, and 6 could accordingly be explained by elevated concentrations of particulate matter ( $\text{PM}_{\text{total}}$ ), indicating that PBM dominated RM dry deposition during these weeks (Figure S2 of the Supporting Information). The inconsistency in weeks 10, 11, and 12, however, was likely associated with elevated RM dry deposition velocities ( $0.47 \text{ cm s}^{-1}$ ), given the low PBM concentrations, as compared to the other weeks ( $0.25 \text{ cm s}^{-1}$ ) that are not reproduced by the Aerohead measurements. It is likely that Hg–N RM compounds were advected on particles, especially during weeks 1 and 6 when the absolute amount of Hg–N RM compounds was elevated (Figure 2a). During the entire campaign, though, the ammonium ( $\text{NH}_4^+$ ) and nitrate ( $\text{NO}_3^-$ ) aerosol concentrations were at least 3 orders of magnitude higher compared to the concentrations of Hg–N compounds. This indicates that RM production and transformation of Hg–N compounds were not directly linked to advection of particulate nitrogen compounds, which is consistent with a predominant gas-phase oxidation of the RM precursor by  $\text{NO}_2$  in the FT.<sup>84</sup>

**3.6. Implications.** Arctic RM concentrations analyzed on CEM and PES were higher than Tekran RM during all weeks of measurements. That the Tekran system significantly underestimated RM concentrations in the Arctic was surprising because one would expect that most of the RM would be Br and Cl compounds, and given the efficiency of the KCl denuder, it should be 1.2–1.3 times lower, as demonstrated by Huang et al.<sup>21</sup> However, experiments by Huang et al.<sup>21</sup> were performed in clean air, whereas the measurements in the Arctic were of ambient air, indicating the impact of some aspect of atmospheric chemistry (e.g.,  $\text{O}_3$ ) on retention of GOM compounds. The difference between RM concentrations was large during the AMDE season (mainly April and May) and became small when the RM concentrations decreased in the summer. In general,  $\text{RM}_{\text{TK}}$  showed a significant, but not strong, correlation ( $r^2 < 0.6$ ) with  $\text{RM}_{\text{CEM}}$  and  $\text{RM}_{\text{PES}}$ . Bias in denuder-based Tekran quantification of GOM could not be corrected, as was suggested for the Pic du Midi high-altitude site in the Pyrenees, France.<sup>25</sup> The bias in Arctic RM concentration measurements between manual and automated methods must be addressed not only during AMDEs but with multi-seasonal sampling campaigns at sites such as Alert in Canada, where Tekran systems are also operated year round.

RM compound-specific deposition velocity estimates provide the way for more accurate RM dry deposition estimates. However, as stated by Gustin et al.,<sup>63</sup> the determination of RM compounds could be improved (1) using a new thermal desorption surface, because the nylon membranes underestimate RM concentrations (by 50% in this study), and (2) identifying the exact chemistry of RM compounds by developing a mass spectrometry method.

The RM dry deposition model revealed higher fluxes when using the RMAS data compared to Tekran data, suggesting a 5.6 times larger input of RM to Arctic ecosystems. In the Ny-Ålesund area, RM dry deposition ( $1.9 \mu\text{g m}^{-2}$  from March 27 to July 24, 2019) was the dominant Hg deposition pathway, exceeding mean annual wet deposition ranging from 0.8 to  $1.7 \mu\text{g m}^{-2} \text{ year}^{-1}$  measured between 2012 and 2015.<sup>82</sup>

If we accept the assumption that dry deposition measurements made by the Aerohead system are accurate for GOM

and measurements performed with RMAS are accurate for RM, our results demonstrate that RM bound to particles constituted 46% of deposited Hg; this also assumes that RM dry deposition occurs homogeneously and independently of different boundary layer conditions at Zeppelin. In fact, large particles of  $>PM_{2.5}$  (not analyzed by the Tekran) contributed 70% to the total PM concentration (Figure S2 of the Supporting Information). This indicates that a dominant portion of RM was associated with large particles ( $>PM_{2.5}$ ), likely marine aerosols. Our study showed that RM dry deposition estimates during the 2019 AMDE season at Zeppelin and potentially elsewhere in the Arctic were likely higher than previously assumed and reported. This has implications for the amount of Hg cycling between the atmosphere and Arctic ecosystems.

## ■ ASSOCIATED CONTENT

### SI Supporting Information

The Supporting Information is available free of charge at <https://pubs.acs.org/doi/10.1021/acsearthspacechem.1c00299>.

Details on automated (section S1) and manual (section S2) RM sampling and analysis, overview of the measured RM concentrations (section S3), thermal desorption procedure and profiles (section S4), back-trajectory modeling (section S5), and dry deposition modeling (section S6) (PDF)

## ■ AUTHOR INFORMATION

### Corresponding Author

**Stefan Osterwalder** – Institut des Géosciences de l'Environnement (IGE), Université Grenoble Alpes, Centre National de la Recherche Scientifique (CNRS), Institut de Recherche pour le Développement (IRD), Institut Polytechnique de Grenoble (Grenoble INP), 38400 Saint-Martin-d'Hères, France; Institute of Agricultural Sciences, ETH Zurich, 8092 Zurich, Switzerland; [orcid.org/0000-0001-8775-0813](https://orcid.org/0000-0001-8775-0813); Email: [stefan.osterwalder@usys.ethz.ch](mailto:stefan.osterwalder@usys.ethz.ch)

### Authors

**Sarah M. Dunham-Cheatham** – Department of Natural Resources and Environmental Sciences, University of Nevada, Reno, Nevada 89557, United States; [orcid.org/0000-0002-2281-1686](https://orcid.org/0000-0002-2281-1686)

**Beatriz Ferreira Araujo** – Centre National de la Recherche Scientifique (CNRS), Institut de Recherche pour le Développement (IRD), Géosciences Environnement Toulouse (GET), Université Paul Sabatier Toulouse III, 31400 Toulouse, France

**Olivier Magand** – Institut des Géosciences de l'Environnement (IGE), Université Grenoble Alpes, Centre National de la Recherche Scientifique (CNRS), Institut de Recherche pour le Développement (IRD), Institut Polytechnique de Grenoble (Grenoble INP), 38400 Saint-Martin-d'Hères, France

**Jennie L. Thomas** – Institut des Géosciences de l'Environnement (IGE), Université Grenoble Alpes, Centre National de la Recherche Scientifique (CNRS), Institut de Recherche pour le Développement (IRD), Institut Polytechnique de Grenoble (Grenoble INP), 38400 Saint-Martin-d'Hères, France

**Foteini Baladima** – Institut des Géosciences de l'Environnement (IGE), Université Grenoble Alpes, Centre

National de la Recherche Scientifique (CNRS), Institut de Recherche pour le Développement (IRD), Institut Polytechnique de Grenoble (Grenoble INP), 38400 Saint-Martin-d'Hères, France

**Katrine Aspmo Pfaffhuber** – Norwegian Institute for Air Research, 2007 Kjeller, Norway

**Torunn Berg** – Department of Chemistry, Norwegian University of Science and Technology, 7491 Trondheim, Norway

**Lei Zhang** – School of the Environment, Nanjing University, Nanjing, Jiangsu 210023, People's Republic of China;

[orcid.org/0000-0003-2796-6043](https://orcid.org/0000-0003-2796-6043)

**Jiaoyan Huang** – Sonoma Technology, Petaluma, California 94954, United States

**Aurélien Dommergue** – Institut des Géosciences de l'Environnement (IGE), Université Grenoble Alpes, Centre National de la Recherche Scientifique (CNRS), Institut de Recherche pour le Développement (IRD), Institut Polytechnique de Grenoble (Grenoble INP), 38400 Saint-Martin-d'Hères, France

**Jeroen E. Sonke** – Centre National de la Recherche Scientifique (CNRS), Institut de Recherche pour le Développement (IRD), Géosciences Environnement Toulouse (GET), Université Paul Sabatier Toulouse III, 31400 Toulouse, France; [orcid.org/0000-0001-7146-3035](https://orcid.org/0000-0001-7146-3035)

**Mae Sexauer Gustin** – Department of Natural Resources and Environmental Sciences, University of Nevada, Reno, Nevada 89557, United States; [orcid.org/0000-0002-9306-2037](https://orcid.org/0000-0002-9306-2037)

Complete contact information is available at:

<https://pubs.acs.org/doi/10.1021/acsearthspacechem.1c00299>

### Funding

This research was funded by the French Polar Institute IPEV (Programme 1207 MESSI) and the EC H2020 ERA-PLANET (Grant 689443) iGOSP and iCUPE Programmes. Additional funding was provided by the EC H2020 research and innovation programme GMOS Train under the Marie Skłodowska-Curie grant agreement no. 860497. The project also received funding from the Swiss National Science Foundation (SNSF) Project P400P2\_180796 and the National Science Foundation (NSF) Project I700711.

### Notes

The authors declare no competing financial interest. Data Availability: A detailed model description is provided in [https://github.com/JiaoyanHuang/Dry\\_Depo\\_multi\\_res\\_model](https://github.com/JiaoyanHuang/Dry_Depo_multi_res_model). Raw data on thermal desorption and peak deconvolution procedures or from back-trajectory modeling are available upon request.

## ■ ACKNOWLEDGMENTS

The authors thank the following people for assistance in the field and laboratory: Laure Laffont from Géosciences Environnement Toulouse (GET), Ove Hermansen and Are Bäcklund from the Norwegian Institute for Air Research (NILU), Christelle Guesnon from the Norwegian Polar Institute (NPI), and all personnel from Institut Polaire Paul Emile Victor (IPEV) and Alfred Wegener Institute (AWI) for Polar and Marine Research. The authors acknowledge Hans-Werner Jacobi from Université Grenoble Alpes and Julia Boike, Christian Lehr, and Siegrid Debatin from AWI for providing snow depth data. The authors are grateful to Paul Zieger from Stockholm University (SU) for providing PM data from

Zeppelin. The authors thank Wenche Aas (NILU) for making data on particulate and gaseous nitrogen compounds available. The student assistants from the University of Nevada, Reno lab are acknowledged for their support with membrane digestion and analysis. The authors thank four anonymous reviewers for their comments.

## REFERENCES

- (1) Arctic Monitoring and Assessment Programme (AMAP). *AMAP Assessment 2011: Mercury in the Arctic*; AMAP: Oslo, Norway, 2011.
- (2) Douglas, T. A.; Loseto, L. L.; Macdonald, R. W.; Outridge, P.; Dommergue, A.; Poulain, A.; Amyot, M.; Barkay, T.; Berg, T.; Chételat, J.; Constant, P.; Evans, M.; Ferrari, C.; Gantner, N.; Johnson, M. S.; Kirk, J.; Kroer, N.; Larose, C.; Lean, D.; Nielsen, T. G.; Poissant, L.; Rognerud, S.; Skov, H.; Sørensen, S.; Wang, F.; Wilson, S.; Zdanowicz, C. M. The fate of mercury in Arctic terrestrial and aquatic ecosystems, a review. *Environ. Chem.* **2012**, *9*, 321–355.
- (3) United Nations Environment Programme (UNEP) Chemicals Branch. *UNEP Minamata Convention on Mercury: Text and Annexes*; UNEP Chemicals Branch: Geneva, Switzerland, 2013; <http://www.mercuryconvention.org> (accessed April 12, 2021).
- (4) Soerensen, A. L.; Jacob, D. J.; Schartup, A. T.; Fisher, J. A.; Lehnher, I.; St. Louis, V. L.; Heimbürger, L.-E.; Sonke, J. E.; Krabbenhoft, D. P.; Sunderland, E. M. A mass budget for mercury and methylmercury in the Arctic Ocean. *Glob. Biogeochem. Cycles* **2016**, *30*, 560–575.
- (5) Dastoor, A. P.; Durnford, D. A. Arctic Ocean: Is It a Sink or a Source of Atmospheric Mercury? *Environ. Sci. Technol.* **2014**, *48*, 1707–1717.
- (6) Schroeder, W. H.; Anlauf, K. G.; Barrie, L. A.; Lu, J. Y.; Steffen, A.; Schneeberger, D. R.; Berg, T. Arctic springtime depletion of mercury. *Nature* **1998**, *394*, 331–332.
- (7) Ariya, P. A.; Dastoor, A. P.; Amyot, M.; Schroeder, W. H.; Barrie, L.; Anlauf, K.; Raofie, F.; Ryzhkov, A.; Davignon, D.; Lalonde, J.; Steffen, A. The Arctic: A sink for mercury. *Tellus, Ser. B* **2004**, *56*, 397–403.
- (8) Skov, H.; Christensen, J. H.; Goodsite, M. E.; Heidam, N. Z.; Jensen, B.; Wählin, P.; Geernaert, G. Fate of elemental mercury in the arctic during atmospheric mercury depletion episodes and the load of atmospheric mercury to the arctic. *Environ. Sci. Technol.* **2004**, *38*, 2373–2382.
- (9) Lindberg, S. E.; Brooks, S.; Lin, C.-J.; Scott, K. J.; Landis, M. S.; Stevens, R. K.; Goodsite, M. E.; Richter, A. Dynamic oxidation of gaseous mercury in the arctic troposphere at polar sunrise. *Environ. Sci. Technol.* **2002**, *36*, 1245–1256.
- (10) Steffen, A.; Douglas, T.; Amyot, M.; Ariya, P.; Aspmo, K.; Berg, T.; Bottenheim, J.; Brooks, S.; Cobbett, F.; Dastoor, A.; Dommergue, A.; Ebinghaus, R.; Ferrari, C.; Gardfeldt, K.; Goodsite, M. E.; Lean, D.; Poulain, A. J.; Scherz, C.; Skov, H.; Sommar, J.; Temme, C. A synthesis of atmospheric mercury depletion event chemistry in the atmosphere and snow. *Atmos. Chem. Phys.* **2008**, *8*, 1445–1482.
- (11) Wang, S.; McNamara, S. M.; Moore, C. W.; Obrist, D.; Steffen, A.; Shepson, P. B.; Staebler, R. M.; Raso, A. R. W.; Pratt, K. A. Direct detection of atmospheric atomic bromine leading to mercury and ozone depletion. *Proc. Natl. Acad. Sci. U. S. A.* **2019**, *116*, 14479–14484.
- (12) Obrist, D.; Agnan, Y.; Jiskra, M.; Olson, C. L.; Colegrove, D. P.; Hueber, J.; Moore, C. W.; Sonke, J. E.; Helmig, D. Tundra uptake of atmospheric elemental mercury drives Arctic mercury pollution. *Nature* **2017**, *547*, 201–204.
- (13) Dommergue, A.; Larose, C.; Faïn, X.; Clarisse, O.; Foucher, D.; Hintelmann, H.; Schneider, D.; Ferrari, C. P. Deposition of Mercury Species in the Ny-Ålesund Area (79°N) and Their Transfer during Snowmelt. *Environ. Sci. Technol.* **2010**, *44*, 901–907.
- (14) Steffen, A.; Bottenheim, J.; Cole, A.; Ebinghaus, R.; Lawson, G.; Leaitch, W. R. Atmospheric mercury speciation and mercury in snow over time at Alert, Canada. *Atmos. Chem. Phys.* **2014**, *14*, 2219–2231.
- (15) Kamp, J.; Skov, H.; Jensen, B.; Sørensen, L. L. Fluxes of gaseous elemental mercury (GEM) in the High Arctic during atmospheric mercury depletion events (AMDEs). *Atmos. Chem. Phys.* **2018**, *18*, 6923–6938.
- (16) Jiskra, M.; Sonke, J. E.; Agnan, Y.; Helmig, D.; Obrist, D. Insights from mercury stable isotopes on terrestrial–atmosphere exchange of Hg(0) in the Arctic tundra. *Biogeosciences* **2019**, *16*, 4051–4064.
- (17) Gustin, M. S.; Huang, J.; Miller, M. B.; Peterson, C.; Jaffe, D. A.; Ambrose, J.; Finley, B. D.; Lyman, S. N.; Call, K.; Talbot, R.; Feddersen, D.; Mao, H.; Lindberg, S. E. Do We Understand What the Mercury Speciation Instruments Are Actually Measuring? Results of RAMIX. *Environ. Sci. Technol.* **2013**, *47*, 7295–7306.
- (18) Gustin, M. S.; Amos, H. M.; Huang, J.; Miller, M. B.; Heidecorn, K. Measuring and modeling mercury in the atmosphere: A critical review. *Atmos. Chem. Phys.* **2015**, *15*, 5697–5713.
- (19) Gustin, M. S.; Dunham-Cheatham, S. M.; Zhang, L. Comparison of 4 Methods for Measurement of Reactive, Gaseous Oxidized, and Particulate Bound Mercury. *Environ. Sci. Technol.* **2019**, *53*, 14489–14495.
- (20) Gustin, M. S.; Dunham-Cheatham, S. M.; Zhang, L.; Lyman, S.; Choma, N.; Castro, M. Use of Membranes and Detailed HYSPLIT Analyses to Understand Atmospheric Particulate, Gaseous Oxidized, and Reactive Mercury Chemistry. *Environ. Sci. Technol.* **2021**, *55*, 893–901.
- (21) Huang, J.; Miller, M. B.; Weiss-Penzias, P.; Gustin, M. S. Comparison of Gaseous Oxidized Hg Measured by KCl-Coated Denuders, and Nylon and Cation Exchange Membranes. *Environ. Sci. Technol.* **2013**, *47*, 7307–7316.
- (22) Huang, J.; Miller, M. B.; Edgerton, E.; Gustin, M. S. Use of criteria pollutants, active and passive mercury sampling, and receptor modeling to understand the chemical forms of gaseous oxidized mercury in Florida. *Atmos. Chem. Phys. Discuss.* **2015**, 12069–12105.
- (23) McClure, C. D.; Jaffe, D. A.; Edgerton, E. S. Evaluation of the KCl Denuder Method for Gaseous Oxidized Mercury using HgBr<sub>2</sub> at an In-Service AMNet Site. *Environ. Sci. Technol.* **2014**, *48*, 11437–11444.
- (24) Luippold, A.; Gustin, M. S.; Dunham-Cheatham, S. M.; Castro, M.; Luke, W.; Lyman, S.; Zhang, L. Use of Multiple Lines of Evidence to Understand Reactive Mercury Concentrations and Chemistry in Hawai'i, Nevada, Maryland, and Utah, USA. *Environ. Sci. Technol.* **2020**, *54*, 7922–7931.
- (25) Maruszczak, N.; Sonke, J. E.; Fu, X.; Jiskra, M. Tropospheric GOM at the Pic du Midi Observatory—Correcting bias in denuder based observations. *Environ. Sci. Technol.* **2017**, *51*, 863–869.
- (26) Lynam, M. M.; Keeler, G. J. Artifacts associated with the measurement of particulate mercury in an urban environment: The influence of elevated ozone concentrations. *Atmos. Environ.* **2005**, *39*, 3081–3088.
- (27) Malcolm, E. G.; Keeler, G. J. Evidence for a sampling artifact for particulate-phase mercury in the marine atmosphere. *Atmos. Environ.* **2007**, *41*, 3352–3359.
- (28) Rutter, A. P.; Hanford, K. L.; Zwiers, J. T.; Perillo-Nicholas, A. L.; Schauer, J. J.; Olson, M. L. Evaluation of an offline method for the analysis of atmospheric reactive gaseous mercury and particulate mercury. *J. Air Waste Manage. Assoc.* **2008**, *58*, 377–383.
- (29) Kos, G.; Ryzhkov, A.; Dastoor, A.; Narayan, J.; Steffen, A.; Ariya, P. A.; Zhang, L. Evaluation of discrepancy between measured and modelled oxidized mercury species. *Atmos. Chem. Phys.* **2013**, *13*, 4839–4863.
- (30) Talbot, R.; Mao, H.; Feddersen, D.; Smith, M.; Kim, S. Y.; Sive, B.; Haase, K.; Ambrose, J.; Zhou, Y.; Russo, R. Comparison of Particulate Mercury Measured with Manual and Automated Methods. *Atmosphere* **2011**, *2*, 1–20.
- (31) Feddersen, D. M.; Talbot, R.; Mao, H.; Sive, B. C. Size distribution of particulate mercury in marine and coastal atmospheres. *Atmos. Chem. Phys.* **2012**, *12*, 10899–10909.

- (32) Luippold, A.; Gustin, M. S.; Dunham-Cheatham, S. M.; Zhang, L. Improvement of quantification and identification of atmospheric reactive mercury. *Atmos. Environ.* **2020**, *224*, 117307.
- (33) Lyman, S. N.; Gustin, M. S.; Prestbo, E. M.; Marsik, F. J. Estimation of Dry Deposition of Atmospheric Mercury in Nevada by Direct and Indirect Methods. *Environ. Sci. Technol.* **2007**, *41*, 1970–1976.
- (34) Lyman, S. N.; Gustin, M. S.; Prestbo, E. M.; Kilner, P. I.; Edgerton, E.; Hartsell, B. Testing and Application of Surrogate Surfaces for Understanding Potential Gaseous Oxidized Mercury Dry Deposition. *Environ. Sci. Technol.* **2009**, *43*, 6235–6241.
- (35) Sexauer Gustin, M.; Weiss-Penzias, P. S.; Peterson, C. Investigating sources of gaseous oxidized mercury in dry deposition at three sites across Florida, USA. *Atmos. Chem. Phys.* **2012**, *12*, 9201–9219.
- (36) Huang, J.; Miller, M. B.; Edgerton, E.; Sexauer Gustin, M. Deciphering potential chemical compounds of gaseous oxidized mercury in Florida, USA. *Atmos. Chem. Phys.* **2017**, *17*, 1689–1698.
- (37) Zhang, L.; Brook, J. R.; Vet, R. A revised parameterization for gaseous dry deposition in air-quality models. *Atmos. Chem. Phys.* **2003**, *3*, 2067–2082.
- (38) Berg, T.; Bartnicki, J.; Munthe, J.; Lattila, H.; Hrehoruk, J.; Mazur, A. Atmospheric mercury species in the European Arctic: Measurements and modelling. *Atmos. Environ.* **2001**, *35*, 2569–2582.
- (39) Berg, T.; Pfaffhuber, K. A.; Cole, A. S.; Engelsens, O.; Steffen, A. Ten-year trends in atmospheric mercury concentrations, meteorological effects and climate variables at Zeppelin, Ny-Ålesund. *Atmos. Chem. Phys.* **2013**, *13*, 6575–6586.
- (40) Berg, T.; Sekkesæter, S.; Steinnes, E.; Valdal, A.-K.; Wibetoe, G. Springtime depletion of mercury in the European Arctic as observed at Svalbard. *Sci. Total Environ.* **2003**, *304*, 43–51.
- (41) Aspmo, K.; Gauchard, P.-A.; Steffen, A.; Temme, C.; Berg, T.; Bahlmann, E.; Banic, C.; Dommergue, A.; Ebinghaus, R.; Ferrari, C.; Pirrone, N.; Sprovieri, F.; Wibetoe, G. Measurements of atmospheric mercury species during an international study of mercury depletion events at Ny-Ålesund, Svalbard, spring 2003. How reproducible are our present methods? *Atmos. Environ.* **2005**, *39*, 7607–7619.
- (42) Gauchard, P.-A.; Aspmo, K.; Temme, C.; Steffen, A.; Ferrari, C.; Berg, T.; Ström, J.; Kaleschke, L.; Dommergue, A.; Bahlmann, E.; Magand, O.; Planchon, F.; Ebinghaus, R.; Banic, C.; Nagorski, S.; Baussand, P.; Boutron, C. Study of the origin of atmospheric mercury depletion events recorded in Ny-Ålesund, Svalbard, spring 2003. *Atmos. Environ.* **2005**, *39*, 7620–7632.
- (43) Sprovieri, F.; Pirrone, N.; Landis, M. S.; Stevens, R. K. Oxidation of Gaseous Elemental Mercury to Gaseous Divalent Mercury during 2003 Polar Sunrise at Ny-Ålesund. *Environ. Sci. Technol.* **2005**, *39*, 9156–9165.
- (44) Sprovieri, F.; Pirrone, N.; Landis, M. S.; Stevens, R. K. Atmospheric mercury behavior at different altitudes at Ny-Ålesund during Spring 2003. *Atmos. Environ.* **2005**, *39*, 7646–7656.
- (45) Sommar, J.; Wängberg, I.; Berg, T.; Gårdfeldt, K.; Munthe, J.; Richter, A.; Urba, A.; Wittrock, F.; Schroeder, W. H. Circumpolar transport and air-surface exchange of atmospheric mercury at Ny-Ålesund (79° N), Svalbard, spring 2002. *Atmos. Chem. Phys.* **2007**, *7*, 151–166.
- (46) Ferrari, C. P.; Padova, C.; Fain, X.; Gauchard, P.-A.; Dommergue, A.; Aspmo, K.; Berg, T.; Cairns, W.; Barbante, C.; Cescon, P.; Kaleschke, L.; Richter, A.; Wittrock, F.; Boutron, C. Atmospheric mercury depletion event study in Ny-Alesund (Svalbard) in spring 2005. Deposition and transformation of Hg in surface snow during springtime. *Sci. Total Environ.* **2008**, *397*, 167–177.
- (47) Steen, A. O.; Berg, T.; Dastoor, A. P.; Durnford, D. A.; Engelsens, O.; Hole, L. R.; Pfaffhuber, K. A. Natural and anthropogenic atmospheric mercury in the European Arctic: A fractionation study. *Atmos. Chem. Phys.* **2011**, *11*, 6273–6284.
- (48) Angot, H.; Dastoor, A.; De Simone, F.; Gårdfeldt, K.; Gencarelli, C. N.; Hedgcock, I. M.; Langer, S.; Magand, O.; Mastromonaco, M. N.; Nordstrøm, C.; Pfaffhuber, K. A.; Pirrone, N.; Ryjkov, A.; Selin, N. E.; Skov, H.; Song, S.; Sprovieri, F.; Steffen, A.; Toyota, K.; Travnikov, O.; Yang, X.; Dommergue, A. Chemical cycling and deposition of atmospheric mercury in polar regions: Review of recent measurements and comparison with models. *Atmos. Chem. Phys.* **2016**, *16*, 10735–10763.
- (49) Landis, M. S.; Stevens, R. K.; Schaedlich, F.; Prestbo, E. M. Development and Characterization of an Annular Denuder Methodology for the Measurement of Divalent Inorganic Reactive Gaseous Mercury in Ambient Air. *Environ. Sci. Technol.* **2002**, *36*, 3000–3009.
- (50) Steffen, A.; Scherz, T.; Olson, M.; Gay, D.; Blanchard, P. A comparison of data quality control protocols for atmospheric mercury speciation measurements. *J. Environ. Monit.* **2012**, *14*, 752–765.
- (51) D'Amore, F.; Bencardino, M.; Cinnirella, S.; Sprovieri, F.; Pirrone, N. Data quality through a web-based QA/QC system: Implementation for atmospheric mercury data from the global mercury observation system. *Environ. Sci.: Processes Impacts* **2015**, *17*, 1482–1491.
- (52) Enrico, M.; Le Roux, G.; Maruszczak, N.; Heimbürger, L.-E.; Claustres, A.; Fu, X.; Sun, R.; Sonke, J. E. Atmospheric mercury transfer to peat bogs dominated by gaseous elemental mercury dry deposition. *Environ. Sci. Technol.* **2016**, *50*, 2405–2412.
- (53) Dunham-Cheatham, S. M.; Lyman, S.; Gustin, M. S. Evaluation of sorption surface materials for reactive mercury compounds. *Atmos. Environ.* **2020**, *242*, 117836.
- (54) Miller, M. B.; Dunham-Cheatham, S. M.; Gustin, M. S.; Edwards, G. C. Evaluation of cation exchange membrane performance under exposure to high Hg<sup>0</sup> and HgBr<sub>2</sub> concentrations. *Atmos. Meas. Tech.* **2019**, *12*, 1207–1217.
- (55) Biester, H.; Scholz, C. Determination of Mercury Binding Forms in Contaminated Soils: Mercury Pyrolysis versus Sequential Extractions. *Environ. Sci. Technol.* **1997**, *31*, 233–239.
- (56) Stein, A. F.; Draxler, R. R.; Rolph, G. D.; Stunder, B. J. B.; Cohen, M. D.; Ngan, F. NOAA's HYSPLIT Atmospheric Transport and Dispersion Modeling System. *Bull. Am. Meteorol. Soc.* **2015**, *96*, 2059–2077.
- (57) Hersbach, H.; Bell, B.; Berrisford, P.; Hirahara, S.; Horányi, A.; Muñoz-Sabater, J.; Nicolas, J.; Peubey, C.; Radu, R.; Schepers, D.; Simmons, A.; Soci, C.; Abdalla, S.; Abellan, X.; Balsamo, G.; Bechtold, P.; Biavati, G.; Bidlot, J.; Bonavita, M.; Chiara, G. D.; Dahlgren, P.; Dee, D.; Diamantakis, M.; Dragani, R.; Flemming, J.; Forbes, R.; Fuentes, M.; Geer, A.; Haimberger, L.; Healy, S.; Hogan, R. J.; Hólm, E.; Janisková, M.; Keeley, S.; Laloyaux, P.; Lopez, P.; Lupu, C.; Radnoti, G.; Rosnay, P.; de Rozum, I.; Vamborg, F.; Villaume, S.; Thépaut, J.-N. The ERA5 global reanalysis. *Q. J. R. Meteorol. Soc.* **2020**, *146*, 1999–2049.
- (58) Boike, J.; Juszak, I.; Lange, S.; Chadburn, S.; Burke, E. J.; Overduin, P. P.; Roth, K.; Ippisch, O.; Bornemann, N.; Stern, L.; Gouttevin, I.; Hauber, E.; Westermann, S. Measurements in soil and air at Bayelva Station. Supplement to: Boike, J et al. (2018): A 20-year record (1998–2017) of permafrost, active layer and meteorological conditions at a high Arctic permafrost research site (Bayelva, Spitsbergen). *Earth Syst. Sci. Data* **2018**, *10*, 355–390.
- (59) Norwegian Institute for Air Research (NILU). *European Monitoring and Evaluation Programme (EMEP) Manual for Sampling and Chemical Analysis*; NILU: Kjeller, Norway, 2001; EMEP Report 1/95, <https://projects.nilu.no/ccc/manual/index.html> (accessed April 12, 2021).
- (60) Hirdman, D.; Aspmo, K.; Burkhart, J. F.; Eckhardt, S.; Sodemann, H.; Stohl, A. Transport of mercury in the Arctic atmosphere: Evidence for a spring-time net sink and summer-time source. *Geophys. Res. Lett.* **2009**, *36*, 36.
- (61) Fisher, J. A.; Jacob, D. J.; Soerensen, A. L.; Amos, H. M.; Steffen, A.; Sunderland, E. M. Riverine source of Arctic Ocean mercury inferred from atmospheric observations. *Nat. Geosci.* **2012**, *5*, 499–504.
- (62) Sonke, J. E.; Teisserenc, R.; Heimbürger-Boavida, L.-E.; Petrova, M. V.; Maruszczak, N.; Le Dantec, T.; Chupakov, A. V.; Li, C.; Thackray, C. P.; Sunderland, E. M.; Tananaev, N.; Pokrovsky, O. S. Eurasian river spring flood observations support net Arctic Ocean

mercury export to the atmosphere and Atlantic Ocean. *Proc. Natl. Acad. Sci. U. S. A.* **2018**, *115*, E11586–E11594.

(63) Gustin, M. S.; Dunham-Cheatham, S. M.; Huang, J.; Lindberg, S.; Lyman, S. N. Development of an Understanding of Reactive Mercury in Ambient Air: A Review. *Atmosphere* **2021**, *12*, 73.

(64) Horowitz, H. M.; Jacob, D. J.; Zhang, Y.; Dibble, T. S.; Slemr, F.; Amos, H. M.; Schmidt, J. A.; Corbitt, E. S.; Marais, E. A.; Sunderland, E. M. A new mechanism for atmospheric mercury redox chemistry: Implications for the global mercury budget. *Atmos. Chem. Phys.* **2017**, *17*, 6353–6371.

(65) Peleg, M.; Tas, E.; Obrist, D.; Matveev, V.; Moore, C.; Gabay, M.; Luria, M. Observational Evidence for Involvement of Nitrate Radicals in Nighttime Oxidation of Mercury. *Environ. Sci. Technol.* **2015**, *49*, 14008–14018.

(66) Jiao, Y.; Dibble, T. S. First kinetic study of the atmospherically important reactions  $\text{BrHg} + \text{NO}_2$  and  $\text{BrHg} + \text{HO}_2$ . *Phys. Chem. Chem. Phys.* **2017**, *19*, 1826–1838.

(67) Lam, K. T.; Wilhelmson, C. J.; Schwid, A. C.; Jiao, Y.; Dibble, T. S. Computational Study on the Photolysis of  $\text{BrHgONO}$  and the Reactions of  $\text{BrHgO}^\bullet$  with  $\text{CH}_4$ ,  $\text{C}_2\text{H}_6$ ,  $\text{NO}$ , and  $\text{NO}_2$ : Implications for Formation of  $\text{Hg(II)}$  Compounds in the Atmosphere. *J. Phys. Chem. A* **2019**, *123*, 1637–1647.

(68) Dibble, T. S.; Zelig, M. J.; Mao, H. Thermodynamics of reactions of  $\text{ClHg}$  and  $\text{BrHg}$  radicals with atmospherically abundant free radicals. *Atmos. Chem. Phys.* **2012**, *12*, 10271–10279.

(69) Toyota, K.; McConnell, J. C.; Lupu, A.; Neary, L.; McLinden, C. A.; Richter, A.; Kwok, R.; Semeniuk, K.; Kaminski, J. W.; Gong, S.-L.; Jarosz, J.; Chipperfield, M. P.; Sioris, C. E. Analysis of reactive bromine production and ozone depletion in the Arctic boundary layer using 3-D simulations with GEM-AQ: Inference from synoptic-scale patterns. *Atmos. Chem. Phys.* **2011**, *11*, 3949–3979.

(70) Yang, X.; Pyle, J. A.; Cox, R. A. Sea salt aerosol production and bromine release: Role of snow on sea ice. *Geophys. Res. Lett.* **2008**, *35*, 35.

(71) Huang, J.; Jaeglé, L.; Chen, Q.; Alexander, B.; Sherwen, T.; Evans, M. J.; Theys, N.; Choi, S. Evaluating the impact of blowing snow sea salt aerosol on springtime  $\text{BrO}$  and  $\text{O}_3$  in the Arctic. *Atmos. Chem. Phys.* **2020**, *20*, 7335–7358.

(72) Simpson, W. R.; Brown, S. S.; Saiz-Lopez, A.; Thornton, J. A.; von Glasow, R. Tropospheric Halogen Chemistry: Sources, Cycling, and Impacts. *Chem. Rev.* **2015**, *115*, 4035–4062.

(73) Simpson, W. R.; von Glasow, R.; Riedel, K.; Anderson, P.; Ariya, P.; Bottenheim, J.; Burrows, J.; Carpenter, L. J.; Friess, U.; Goodsite, M. E.; Heard, D.; Hutterli, M.; Jacobi, H. W.; Kaleschke, L.; Neff, B.; Plane, J.; Platt, U.; Richter, A.; Roscoe, H.; Sander, R.; Shepson, P.; Sodeau, J.; Steffen, A.; Wagner, T.; Wolff, E. Halogens and their role in polar boundary-layer ozone depletion. *Atmos. Chem. Phys.* **2007**, *7*, 4375–4418.

(74) Abbatt, J. P. D.; Thomas, J. L.; Abrahamsson, K.; Boxe, C.; Granfors, A.; Jones, A. E.; King, M. D.; Saiz-Lopez, A.; Shepson, P. B.; Sodeau, J.; Toohey, D. W.; Toubin, C.; von Glasow, R.; Wren, S. N.; Yang, X. Halogen activation via interactions with environmental ice and snow in the polar lower troposphere and other regions. *Atmos. Chem. Phys.* **2012**, *12*, 6237–6271.

(75) Foster, K. L.; Plastringer, R. A.; Bottenheim, J. W.; Shepson, P. B.; Finlayson-Pitts, B. J.; Spicer, C. W. The Role of  $\text{Br}_2$  and  $\text{BrCl}$  in Surface Ozone Destruction at Polar Sunrise. *Science* **2001**, *291*, 471–474.

(76) Liao, J.; Huey, L. G.; Liu, Z.; Tanner, D. J.; Cantrell, C. A.; Orlando, J. J.; Flocke, F. M.; Shepson, P. B.; Weinheimer, A. J.; Hall, S. R.; Ullmann, K.; Beine, H. J.; Wang, Y.; Ingall, E. D.; Stephens, C. R.; Hornbrook, R. S.; Apel, E. C.; Riemer, D.; Fried, A.; Mauldin, R. L.; Smith, J. N.; Staebler, R. M.; Neuman, J. A.; Nowak, J. B. High levels of molecular chlorine in the Arctic atmosphere. *Nat. Geosci.* **2014**, *7*, 91–94.

(77) Zhang, L.; Jaffe, D. A. Trends and sources of ozone and sub-micron aerosols at the Mt. Bachelor Observatory (MBO) during 2004–2015. *Atmos. Environ.* **2017**, *165*, 143–154.

(78) Pal, B.; Ariya, P. A. Studies of ozone initiated reactions of gaseous mercury: Kinetics, product studies, and atmospheric implications. *Phys. Chem. Chem. Phys.* **2004**, *6*, 572–579.

(79) Lyman, S. N.; Gustin, M. S.; Prestbo, E. M. A passive sampler for ambient gaseous oxidized mercury concentrations. *Atmos. Environ.* **2010**, *44*, 246–252.

(80) Huang, J.; Lyman, S. N.; Hartman, J. S.; Gustin, M. S. A review of passive sampling systems for ambient air mercury measurements. *Environ. Sci. Process Impacts* **2014**, *16*, 374–392.

(81) Huang, J.; Gustin, M. S. Uncertainties of Gaseous Oxidized Mercury Measurements Using KCl-Coated Denuders, Cation-Exchange Membranes, and Nylon Membranes: Humidity Influences. *Environ. Sci. Technol.* **2015**, *49*, 6102–6108.

(82) Sprovieri, F.; Pirrone, N.; Bencardino, M.; D'Amore, F.; Angot, H.; Barbante, C.; Brunke, E.-G.; Arcega-Cabrera, F.; Cairns, W.; Comero, S.; Diéguez, M. D. C.; Dommergue, A.; Ebinghaus, R.; Feng, X. B.; Fu, X.; Garcia, P. E.; Gawlik, B. M.; Hageström, U.; Hansson, K.; Horvat, M.; Kotnik, J.; Labuschagne, C.; Magand, O.; Martin, L.; Mashyanov, N.; Mkololo, T.; Munthe, J.; Obolkin, V.; Ramirez Islas, M.; Sena, F.; Somerset, V.; Spandow, P.; Vardè, M.; Walters, C.; Wangberg, I.; Weigelt, A.; Yang, X.; Zhang, H. Five-year records of mercury wet deposition flux at GMOS sites in the Northern and Southern hemispheres. *Atmos. Chem. Phys.* **2017**, *17*, 2689–2708.